Control of Quadrotors for Robust Perching and Landing

Daniel Mellinger, Michael Shomin, and Vijay Kumar
GRASP Lab, University of Pennsylvania
[dmel,shomin,kumar]@seas.upenn.edu

While the use of micro unmanned vehicles is steadily increasing, there are currently no viable approaches for perching and holding on to landing pads. We describe the design, control, and planning methodologies to enable perching. Our work builds on an off-the-shelf UAV and motion capture system and addresses (a) the design and fabrication of a claw or gripping mechanism for perching; and (b) planning and control algorithms for perching. We show experimental results illustrating the robustness of our algorithms and the performance envelope for grasping and perching.

Notation

$\mathscr{B}$	Body frame
g	Gravity
I	Moment of inertia matrix about center of mass
L	Distance from center of mass to motor axis
m	Mass of quadrotor
p,q,r	Body frame angular velocity components
$\mathbf{r}$	Position of center of mass of quadrotor
R	Rotation matrix from body to world frame
$\mathscr{W}$	World frame
ϕ,θ,ψ	Roll, pitch, yaw angles
$\mathbf{e}_p,\mathbf{e}_v$	Position and velocity errors
F_i	Force produced by ith propeller
$k_{d,*},k_{p,*}$	Controller gains
k_F	Propeller force constant
k_m	Motor gain
k_M	Propeller moment constant
M_i	Force produced by ith propeller
$\mathbf{r}_T(t)$	Desired trajectory
$\mathbf{x},\mathbf{y},\mathbf{z}_B$	Body frame axes
$\mathbf{x},\mathbf{y},\mathbf{z}_W$	World frame axes
$\psi_T(t)$	Desired yaw angle
ω_h	Nominal angular velocity required to hover
ω_i	Angular velocity of ith propeller
$\Delta\omega_*$	Differential motor speeds

Introduction

The last five years have seen a significant increase in interest in autonomous Micro Unmanned Aerial Vehicles (MAVs) that are between 0.1-0.5 meters in length and 0.1-0.5 kilograms in mass. There are many commercially available MAVs as well as laboratory prototypes in this scale. See, for example, (Refs. 1–5). Because of their ability to fly at low altitudes and because of their size, MAVs have found applications in reconnaissance and surveillance missions as well as search and rescue missions in urban environments.

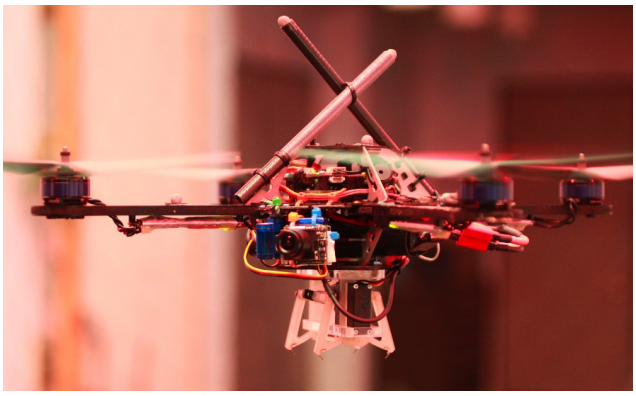

Fig. 1. Quadrotor with gripping mechanism and camera.

While there are many papers (Refs. 2–4, 6, 7) including our own work (Refs. 8, 9) dealing with autonomous flight, our interest here is in the design of hardware and software to support autonomous landing and perching. In applications like persistent surveillance it is necessary for MAVs to operate for long periods of time. Because battery life is limited, it is not feasible for MAVs to remain airborne. It is desirable to develop vehicles that can perch or land at carefully selected positions that offer a good vantage point.

In this paper, we describe a method for quadrotors to robustly land on ledges or horizontal, flat pads. This requires the quadrotor to recognize suitable perching pads, plan paths to the pad, control the relative position and orientation with respect to the pad and then finally grasp the pad with claws. Our focus is on the design of the trajectories, the control of the quadrotor and the perching maneuver. We describe the design of a claw or gripping mechanism that is used to hold onto a surface after landing on it. In a perch and stare mission, when the surveillance task is completed,

Presented at the International Powered Lift Conference, October 5-7, 2010, Philadelphia, PA.

the gripper can release enabling the quadrotor to fly to a new location. In previous work (Ref. 9) we described a control algorithm for perching on a vertical surface. Here we extend that method to robustly perch on a vertical surface.

Experimental Setup

Quadrotor Platform

For our base platform we use the Hummingbird quadrotor sold by Ascending Technologies, GmbH (Ref. 5) shown in Figure 1. This quadrotor has a tip-to-tip wingspan of 55 cm, a height of 8 cm, and weighs about 500 grams including a battery. We chose a quadrotor over a fixed-wing aircraft because it can hover in place so it has an advantage in navigating constrained spaces. The Hummingbird was chosen because it has roughly a 20 minute battery life at hover, can carry 500 grams of payload, and is durable enough to survive most crashes. At the software level, the Hummingbird provides space on an onboard microcontroller for user code.

VICON Motion Capture System

The VICON Motion Capture System provides a position estimate of the quadrotor which is nearly ground truth (Ref. 10). The system can be run at or below 375 Hz and experimental tests show that the standard deviations of position estimates for single static markers are on the order of 50 microns which is well beyond the requirements for flight. The VICON system rarely loses tracking of quadrotors, even during extreme situations such as fast maneuvers (speeds of 3.5 $\frac{\text{m}}{\text{s}}$, accelerations of 15 $\frac{\text{m}}{\text{s}^2}$ and angular speeds of 1000 $\frac{^\circ}{\text{s}}$). In this work the VICON system is used to track the quadrotor as well as the landing and perching surfaces.

Software and Integration

At the core of our software infrastructure is a finite-state machine used for constructing experiments. Each mode of the system consists of closed loop controllers with different objectives or goals. The control software is integrated with the motion capture system and accessed via ROS, an open-source, meta-operating system (Ref. 11) now developed and supported by Willow Garage.

Simulation

It is efficient to design and test control algorithms in simulation before implementation on the physical system. For this reason we developed and characterized a high fidelity dynamic model of the quadrotor described in the next section.

Modeling

Here we describe that the dynamic model of the system that is used for controller development and simulation. The model and controllers were presented in (Ref. 8) and are presented again here for completeness.

Dynamic Model

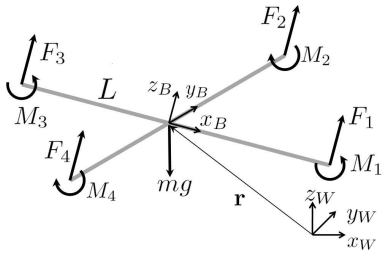

Fig. 2. Coordinate systems and forces/moments acting on the quadrotor frame.

The coordinate systems and free body diagram for the quadrotor are shown in Figure 2. The world frame, $\mathscr{W}$, is defined by axes x_W, y_W, and z_W with z_W pointing upward. The body frame, $\mathscr{B}$, is attached to the center of mass of the quadrotor with x_B coinciding with the preferred forward direction and z_B perpendicular to the plane of the rotors pointing vertically up during perfect hover (see Figure 2). Rotor 1 is on the positive x_B-axis, 2 on the positive y_B-axis, 3 on the negative x_B-axis, 4 on the negative y_B-axis. We use $Z-X-Y$ Euler angles to model the rotation of the quadrotor in the world frame. To get from $\mathscr{W}$ to $\mathscr{B}$, we first rotate about z_W by the yaw angle, ψ, then rotate about the intermediate x-axis by the roll angle, ϕ, and finally rotate about the y_B axis by the pitch angle, θ. The rotation matrix for transforming coordinates from $\mathscr{B}$ to $\mathscr{W}$ is given by

$$R = \begin{bmatrix} c\psi c\theta - s\phi s\psi s\theta & -c\phi s\psi & c\psi s\theta + c\theta s\phi s\psi \\ c\theta s\psi + c\psi s\phi s\theta & c\phi c\psi & s\psi s\theta - c\psi c\theta s\phi \\ -c\phi s\theta & s\phi & c\phi c\theta \end{bmatrix},$$

where $c\theta$ and $s\theta$ denote $\cos(\theta)$ and $\sin(\theta)$, respectively, and similarly for ϕ and ψ. The position vector of the center of mass in the world frame is denoted by $\mathbf{r}$. The forces on the system are gravity, in the $-z_W$ direction, and the forces from each of the rotors, F_i, in the z_B direction. The equations governing the acceleration of the center of mass are

$$m\ddot{\mathbf{r}} = \begin{bmatrix} 0 \\ 0 \\ -mg \end{bmatrix} + R \begin{bmatrix} 0 \\ 0 \\ \Sigma F_i \end{bmatrix}. \tag{1}$$

The components of angular velocity of the robot in the body frame are p, q, and r. These values are related to the derivatives of the roll, pitch, and yaw angles according to

$$\begin{bmatrix} p \\ q \\ r \end{bmatrix} = \begin{bmatrix} c\theta & 0 & -c\phi s\theta \\ 0 & 1 & s\phi \\ s\theta & 0 & c\phi c\theta \end{bmatrix} \begin{bmatrix} \dot{\phi} \\ \dot{\theta} \\ \dot{\psi} \end{bmatrix}.$$

In addition to forces, each rotor produces a moment perpendicular to the plane of rotation of the blade, M_i. Rotors 1 and 3 rotate in the $-z_B$ direction while 2 and 4 rotate in the z_B direction. Since the moment produced on the quadrotor is opposite to the direction of rotation of the blades, M_1 and M_3 act in the z_B direction while M_2 and M_4 act in the $-z_B$ direction. We let L be the distance from the axis of rotation of the rotors to the center of the quadrotor. The moment of inertia matrix referenced to the center of mass along the $x_B - y_B - z_B$ axes, I, is found by building a physically accurate model in SolidWorks. The angular acceleration determined by the Euler equations is

$$I \begin{bmatrix} \dot{p} \\ \dot{q} \\ \dot{r} \end{bmatrix} = \begin{bmatrix} L(F_2 - F_4) \\ L(F_3 - F_1) \\ M_1 - M_2 + M_3 - M_4 \end{bmatrix} - \begin{bmatrix} p \\ q \\ r \end{bmatrix} \times I \begin{bmatrix} p \\ q \\ r \end{bmatrix}. \quad (2)$$

Motor Model

Each rotor has an angular speed ω_i and produces a vertical force F_i according to

$$F_i = k_F \omega_i^2. \quad (3)$$

Experimentation with a fixed rotor at steady-state shows that $k_F \approx 6.11 \times 10^{-8} \frac{N}{rpm^2}$. The rotors also produce a moment according to

$$M_i = k_M \omega_i^2. \quad (4)$$

by matching the performance of the simulation to the real system the constant, k_M, is determined to be about $1.5 \times 10^{-9} \frac{Nm}{rpm^2}$.

The results of a system identification exercise suggest that the rotor speed is related to the commanded speed by a first-order differential equation

$$\dot{\omega}_i = k_m(\omega_i^{des} - \omega_i).$$

This motor gain, k_m, is found to be about $20\,\mathrm{s}^{-1}$ by matching the performance of the simulation to the real system. Experimentation has shown that the desired angular velocities, ω_i^{des}, are limited to a minimum and maximum value of approximately 1200 rpm and 7800 rpm.

Robot Controllers

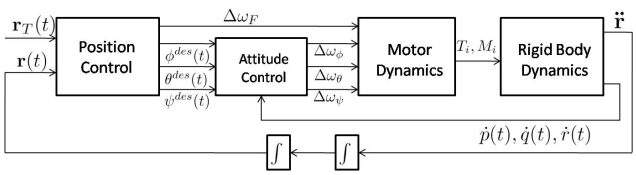

Fig. 3. The nested control loops for position and attitude control.

The control feedback loop is shown in Figure 3. The inner attitude control loop uses onboard accelerometers and gyros to control the roll, pitch, and yaw and runs at approximately 1 kHz (Ref. 2), while the outer position control loop uses estimates of position and velocity of the center of mass to control along the trajectory. Similar nesting of control loops is presented in previous works (Refs. 2–4, 6, 7).

The control law is derived by linearizing the equations of motion and motor models (1 – 4) at an operating point corresponding to the nominal hover state, $\mathbf{r} = \mathbf{r}_0$, $\theta = \phi = 0$, $\psi = \psi_0$, $\dot{\mathbf{r}} = 0$, and $\dot{\phi} = \dot{\theta} = \dot{\psi} = 0$. Here the roll and pitch angles are small and the following approximations hold: $c\phi \approx 1$, $c\theta \approx 1$, $s\phi \approx \phi$, and $s\theta \approx \theta$. For hovering in place the nominal thrusts from the propellers must satisfy

$$F_{i,0} = \frac{mg}{4},$$

and the motor speeds are given by

$$\omega_{i,0} = \omega_h = \sqrt{\frac{mg}{4k_F}}.$$

Attitude Control

We now present an attitude controller designed to control the quadrotor to orientations that are close to the nominal hover state. The desired rotor speeds can be written as a linear combination of four terms as follows

$$\begin{bmatrix} \omega_1^{des} \\ \omega_2^{des} \\ \omega_3^{des} \\ \omega_4^{des} \end{bmatrix} = \begin{bmatrix} 1 & 0 & -1 & 1 \\ 1 & 1 & 0 & -1 \\ 1 & 0 & 1 & 1 \\ 1 & -1 & 0 & -1 \end{bmatrix} \begin{bmatrix} \omega_h + \Delta\omega_F \\ \Delta\omega_\phi \\ \Delta\omega_\theta \\ \Delta\omega_\psi \end{bmatrix}, \quad (5)$$

where the nominal rotor speed required to hover in steady state is ω_h, and the deviations from this nominal vector are $\Delta\omega_F$, $\Delta\omega_\phi$, $\Delta\omega_\theta$, and $\Delta\omega_\psi$. $\Delta\omega_F$ results in a net force along the z_B axis, while $\Delta\omega_\phi$, $\Delta\omega_\theta$, and $\Delta\omega_\psi$ produce moments causing roll, pitch, and yaw, respectively. This is similar to the approach described in (Ref. 2).

We use proportional derivative control with the motor speed differentials as the control inputs

$$\begin{aligned} \Delta\omega_\phi &= k_{p,\phi}(\phi^{des} - \phi) + k_{d,\phi}(p^{des} - p) \\ \Delta\omega_\theta &= k_{p,\theta}(\theta^{des} - \theta) + k_{d,\theta}(q^{des} - q) \\ \Delta\omega_\psi &= k_{p,\psi}(\psi^{des} - \psi) + k_{d,\psi}(r^{des} - r). \end{aligned} \quad (6)$$

Substituting (6) into (5) yields the desired rotor speeds.

Position Control

Here we present two position control methods that use the roll and pitch angles as inputs. The first is a hover controller used for maintaining the position at a desired x, y, and z location. The second is a generalization of the first and tracks three-dimensional trajectories.

Hover Controller Here we use pitch and roll angle to control position in the x_W and y_W plane, $\Delta\omega_\psi$ to control yaw angle, and $\Delta\omega_F$ to control position along z_W. We define $\mathbf{r}_T(t)$ and $\psi_T(t)$ as the trajectory and yaw angle to be tracked. Note that for the hover controller the yaw angle is a constant, $\psi_T(t) = \psi_0$. We use PID feedback on the position error, $e_i = (r_{i,T} - r_i)$, to compute the command accelerations, $\ddot{r}_i^{des}$, as follows

$$\begin{aligned}(\ddot{r}_{i,T} - \ddot{r}_i^{des}) &+ k_{d,i}(\dot{r}_{i,T} - \dot{r}_i) + k_{p,i}(r_{i,T} - r_i) \\ &+ k_{i,i}\int (r_{i,T} - r_i) = 0, \end{aligned} \tag{7}$$

where $\dot{r}_{i,T} = \ddot{r}_{i,T} = 0$ for hover.

We linearize (1) to get the relationship between the desired accelerations and roll and pitch angles. These equations are used to compute the desired roll and pitch angles for the attitude controller and $\Delta\omega_F$ from the desired accelerations

$$\phi^{des} = \frac{1}{g}(\ddot{r}_1^{des}\sin\psi_T - \ddot{r}_2^{des}\cos\psi_T) \tag{8a}$$

$$\theta^{des} = \frac{1}{g}(\ddot{r}_1^{des}\cos\psi_T + \ddot{r}_2^{des}\sin\psi_T) \tag{8b}$$

$$\Delta\omega_F = \frac{m}{8k_F\omega_h}\ddot{r}_3^{des} \tag{8c}$$

.

Note that the position control loop runs at 100 Hz, while the onboard attitude control loop runs at 1 kHz.

3D Trajectory Control The 3D Trajectory Controller is used to follow three-dimensional trajectories with modest accelerations. We define modest accelerations as those for which the small angle assumptions on the roll and pitch angles remain valid. We extend the method described in (Ref. 4) from 2D to 3D trajectories. We first find the closest point on the trajectory, $\mathbf{r}_T$, to the the current position, $\mathbf{r}$. We let the unit tangent vector of the trajectory associated with that closest point be $\hat{\mathbf{t}}$ and the desired velocity vector be $\dot{\mathbf{r}}_T$. The position and velocity errors are defined as

$$\mathbf{e}_p = ((\mathbf{r}_T - \mathbf{r})\cdot\hat{\mathbf{n}})\hat{\mathbf{n}} + ((\mathbf{r}_T - \mathbf{r})\cdot\hat{\mathbf{b}})\hat{\mathbf{b}} \tag{9}$$

and

$$\mathbf{e}_v = \dot{\mathbf{r}}_T - \dot{\mathbf{r}}. \tag{10}$$

The position error is defined in this way to ignore position error in the tangent direction and only consider position error in the normal, $\hat{\mathbf{n}}$, and binormal, $\hat{\mathbf{b}}$, directions. PD feedback of the position and velocity errors is then used to calculate the commanded accelerations

$$\ddot{r}_i^{des} = k_{p,i}e_{i,p} + k_{d,i}e_{i,v} + \ddot{r}_{i,T} \tag{11}$$

Note that the $\ddot{r}_{i,T}$ terms represent feedforward terms on the desired accelerations. These terms can significantly improve performance for trajectories with large accelerations or controllers with soft gains . Finally we use (8a), (8b), and (8c) to compute the desired roll angle, pitch angle, and $\Delta\omega_F$.

Control for Robust Landing

Here we describe a sequence of the controllers from the previous section designed to robustly land on a small horizontal surface. We assume the position and velocity of the quadrotor are available for the feedback controller and the x and y position of the landing location can be sensed with zero mean error. We do not require the exact z height of the landing location to be sensed as it is detected from a change in quadrotor performance. The sensing of an event or the passing of a specified amount of time triggers a change in the controller mode. A diagram illustrating the control strategy is shown in Figure 4. Note that event-triggered transitions are labeled with the event and time-triggered transitions are denoted by clocks.

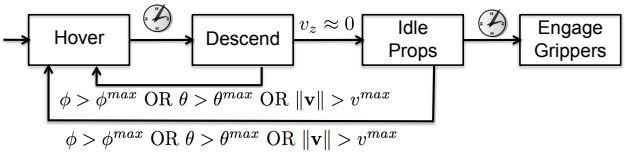

Fig. 4. Control strategy for robust landing.

First, the quadrotor is controlled to **Hover** above the desired landing location. Next it is commanded to **Descend** at a specified velocity. While in the **Descend** mode the quadrotor waits to sense an event before transitioning to the next mode. If an error is sensed the quadrotor is controlled to hover at its original location. If a z velocity close to zero is sensed then the quadrotor has likely made contact with the surface and the quadrotor enters the **Idle Props** mode. If an error is sensed in this mode the quadrotor is commanded to **Hover** at its original location. If no error occurs in some amount of time then the grippers are engaged.

The concept of an error is an important part of this control strategy. Here we sense an error by checking if the roll angle, pitch angle, or velocity are above the threshold values ϕ^{max}, θ^{max}, and v^{max}. These conditions are designed to catch situations when the quadrotor is falling off the desired landing location or when the quadrotor is in free fall because it switched into the **Idle Props** mode when it was not actually on a surface.

Control for Robust Perching

In (Ref. 9) we described a sequence of controllers used to reach a goal state with a specified position, velocity, yaw angle, and pitch angle, with zero angular velocity and roll

angle. This method was used for perching on surfaces of various angles. Here we modify this method to allow for robust perching on vertical surfaces.

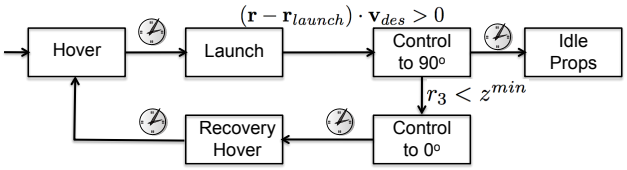

Fig. 5. Control strategy for robust perching on a vertical wall.

During all modes the yaw angle is controlled to be constant. In the **Launch** mode, the robot controls along a 3D line segment at a commanded velocity, $\mathbf{v}_{des}$, towards a launch point, $\mathbf{r}_{launch}$. **Control to 90°** is initiated when the quadrotor passes the plane perpendicular to the desired velocity at the launch point after which the robot's attitude controls to a commanded pitch angle of 90° and a roll angle of zero. At this point if the quadrotor successfully attaches to the vertical surface, the propellers are controlled to idle.

If the quadrotor misses perching on the wall then steps must be taken for the quadrotor to recover. First we must detect that the quadrotor has failed to attach to the wall. We do this by sensing that the quadrotor has dropped below the height where perching is possible, z^{min}. After sensing that the quadrotor has missed the wall, it is sent to the **Control to 0°** mode for a specified time and then to hover at a distance away from the wall with a controller with soft gains and a large basin of attraction. After recovering the quadrotor attempts to perch again.

Gripper

Design

We take inspiration for the gripper from another area with robots grabbing onto planar surfaces; climbing robots. The RISE Robot (Ref. 12) uses compliant microspines to engage with surface asperities on rough surfaces. Utilizing penetration has also been explored for the purpose of scaling vertical surfaces (Ref. 13). Penetration enables large normal forces with respect to shear forces on a surface. This gripper was designed to penetrate surfaces via opposed microspines actuated by a servo motor. Opposed spines allow large shear forces, which in turn allow large normal force.

We designed the gripper with a compliant polymer for many reasons. Firstly, the compliance introduces a restoring force that assists the actuator both in penetration and release from a surface. When the actuator spreads the gripper in preparation for penetration, it imparts potential energy into the gripper's "spring". This nearly doubles the initial penetrating force at the claws. This is very useful, especially for hard wood surfaces. At some point in the penetration, the gripper passes through its equilibrium position and the actuator begins to compress the "spring". Now the compliance is utilized to aid in releasing the gripper. This is useful because the gripper can become stuck in material after remaining embedded for some time. This extra force from the "spring" aids the actuator to free the gripper.

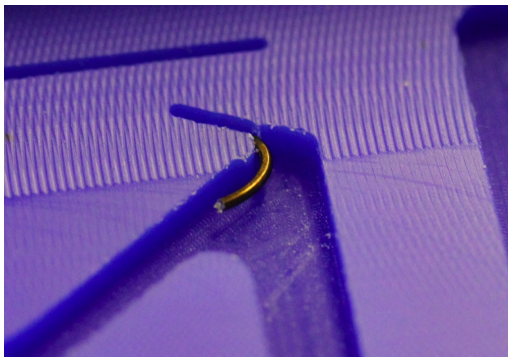

Fig. 6. Locating the hooks in the machinable wax mold.

Manufacturing

Shape Deposition Manufacturing is a method in which Material is deposited in a form that is desirable (Ref. 14). Deposition of the material allows for complicated geometry, large variety of materials, many different materials in a single piece, embedding of other devices of electronics, and fine control of compliance.

We made the main piece of this gripper via Shape Deposition Manufacturing. After designing the piece, a negative mold was milled out of machinable wax. We do this machining via CNC which allows for production of multiple identical grippers. We use machinable wax as it allows for small, precise geometries; fast machining time; and has desirable release properties. The other advantage of wax is that the mold can be reused to produce more grippers.

Location of the hooks in the gripper is essential to the success of the overall design. The angle of attack of the hooks to the surface is especially important. After testing, an angle of 30 degrees with the surface of the material proved to be adequate for engagement as well and supporting normal forces after engagement. The hooks are placed into the molds before pouring the two-part epoxy-resin polymer. Channels are milled out of the mold for the straight shank of the hook. This produces a very consistent angle of attack. The tip of each hook is placed at the end of the channel, providing a consistent length for each claw. This can be seen in Figure 6. This precise locating of the hooks is the main motivation for utilizing Shape Deposition Manufacturing. Embedding the hooks provided an adequate structural integrity, as well as the means for locating the hooks precisely. Because the hooks are small and have no means of mounting, no other method could provide the same advantages.

After machining the mold and locating the hooks, the two-part epoxy-resin polymer from Innovative Polymers is mixed and poured into the mold. The polymer is de-gassed in a vacuum chamber to rid the plastic of micro-bubbles. We then cure the plastic in an oven. The polymer used is Innovative's TP4004. This particular polymer is chosen for its stiffness as well as curing time. The short turn-around time on this particular plastic allows for fast iteration on the design. A one-hour first cure as opposed to a week-long cure time enables more iteration and testing.

After the pieces cure, we combine them with a few laser-cut components as well as an HS-81 micro-hobby servo-motor. This final assembly can be seen in Figure 7. This assembly is attached to the quadrotor via a laser-cut adapter plate. The quadrotor with the gripper can be seen in Figure 1.

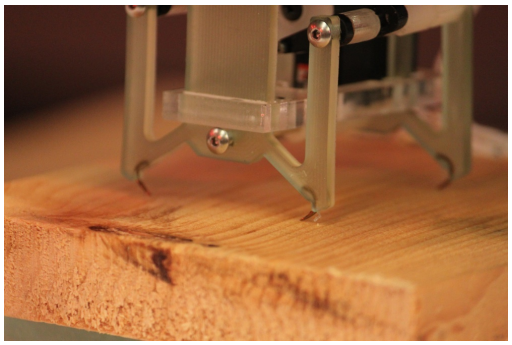

Fig. 7. Full SDM Gripper Assembly.

Camera

A wireless RF Camera was added to the quadrotor for surveilling after perching. We utilize an Airwave AWM687TX RF Wireless Camera. The camera uses a transmission frequency of 5.8 GHz. This was chosen so as not to wash out the the 2.8GHz spectrum which is uses for commanding the quadrotor. The camera is also attached to two HS-55 Hi-Tec Micro Hobby Servos, allowing for panning and tilting. We control this manually via a 6-Channel Futaba RC Receiver. The pan and tilt mechanism allows for much greater visibility and surveillance after landing. The camera and mechanism can be seen in Figure 8. After the quadrotor has landed and engaged the gripper, it can remain there surveilling the vicinity as long as its battery could last. This could conceivably allow for undetected surveillance or a team of quadrotors surveilling an area together. The total weight of the camera, servos, and full gripper mechanism is approximately 140 grams. The maximum capacity of the quadrotor is 1250 grams, while a reasonable payload to maintain maneuverability is about 500 grams. Clearly this package is well within that bound.

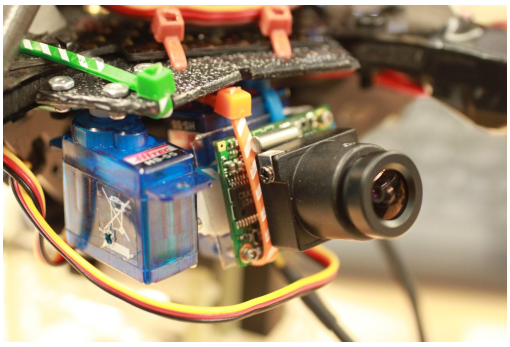

Fig. 8. Camera with Pan and Tilt Mechanism.

Results

Gripper Data

We tested the gripper on multiple surfaces for maximum payload before failure and repeatability. The results can be seen in Figure 9. Each surface was tested 10 times. The error bars represent the standard deviation around the mean failure load. Each failure was due to fracture of the gripped material surface. The maximum payload that can be tested with this equipment is 3 kg. The medium hardness wood, against the grain, never failed at less than 3 kg, and therefore saturated the apparatus. This is why this data shows no standard deviation, as it never failed at this load. The "grain" of the carpet is the directionality of the loops. "Against the Grain" for the carpet indicates the hooks of the gripper piercing perpendicular to the loops. For the cardboard, the "grain" is the directionality of the corrugations. Again, "Against the Grain" corresponds to the hooks being perpendicular to the ripples of the corrugation. The particle board has a random grain direction, and therefore only has one set of data.

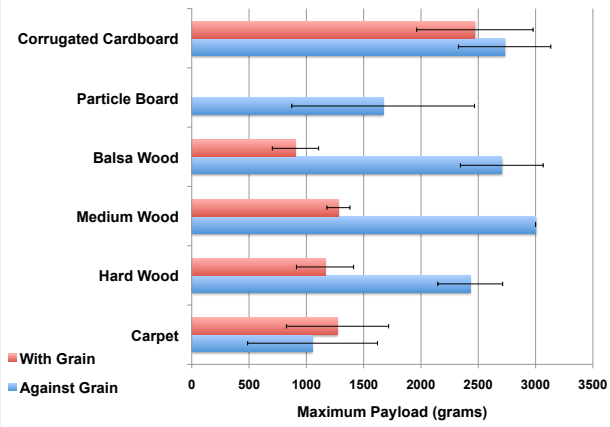

Fig. 9. Maximum Payload of Gripper of Different Surfaces.

Robust Landing

The quadrotor was commanded to land on the wide side of a two-by-four ten times. All ten trials were successful and the standard deviations in the x and y landing locations were both less than 1 cm. The two-by-four was then displaced in various directions from the quadrotor's target location for 40 trials. On all 40 trials the quadrotor successfully recovered to a stable hover. These trials included cases where only two claws made contact with the board as well as cases where all claws completely missed the board. A representative trial is shown in Figure 10. The quadrotor descends until it hits the board and then switches to the idle propellers mode. The quadrotor begins to fall off the board and enters the recovery hover mode after the roll angle exceeds 10°. The quadrotor then recovers to its original position and is ready to perform another attempt at landing.

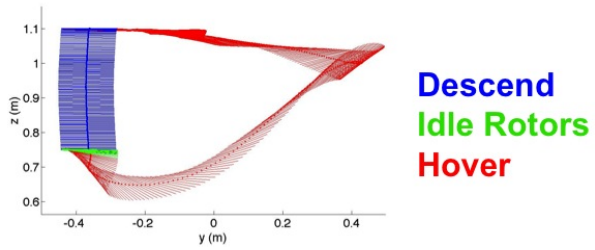

Fig. 10. Recovery from a failed landing attempt on a horizontal surface. Videos of the experiments are available at http://mrsl.grasp.upenn.edu/iplc2010/movie.

Robust Perching

The quadrotor was commanded to perch on a vertical surface for ten trials. In order to guarantee failure no mechanism was placed on the quadrotor to enable attachment. For all ten trials the quadrotor recovered to a stable hover. A representative trial is shown in Figure 11. The quadrotor launches to the wall then controls to a pitch angle of 90°. After failing to attach to the wall the quadrotor is controlled to a pitch angle of 0° and then finally to a stable hover.

Concluding Remarks

This paper makes two key contributions that enable micro unmanned vehicles to grasp/lift objects and perch on window sills or jams. First we described the design and fabrication of a claw or gripping mechanism for grasping and perching. Second, we developed planning and control algorithms for robust perching. Our experimental results demonstrate that our algorithms are robust and the grasping mechanism supports payloads of 1-2 kgs. We also describe the system design which is built from off-the-shelf components.

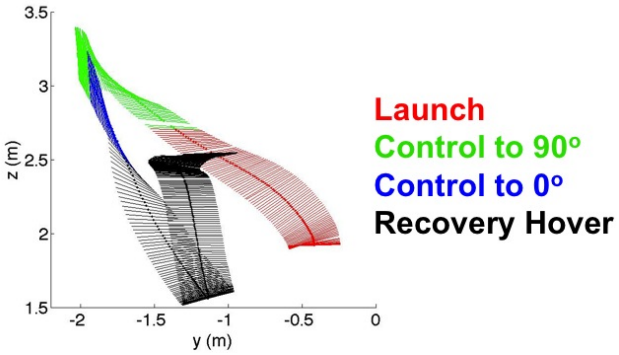

Fig. 11. Recovery from a failed perching attempt on a vertical surface.

While this paper addresses autonomous navigation, landing and perching, it ignores the difficulties with sensing and state estimation. The low-level attitude and position estimation relies on a motion capture system. An important direction of current and ongoing work is the development of a camera-based state estimation and localization system (Ref. 15). We plan to build on this work to incorporate a vision-based recognition system that will automatically identify candidate perching pads.

References

[1]Pines, D. and Bohorquez, F., "Challenges facing future micro air vehicle development," *AIAA Journal of Aircraft*, Vol. 43, (2), 2006, pp. 290–305.

[2]Gurdan, D., Stumpf, J., Achtelik, M., Doth, K., Hirzinger, G., and Rus, D., "Energy-efficient Autonomous Four-rotor Flying Robot Controlled at 1 kHz," Proc. of the IEEE Int. Conf. on Robotics and Automation, April 2007.

[3]Bouabdallah, S., *Design and Control of Quadrotors with Application to Autonomous Flying*, Ph.D. thesis, Ecole Polytechnique Federale de Lausanne, 2007.

[4]Hoffmann, G., Waslander, S., and Tomlin, C., "Quadrotor Helicopter Trajectory Tracking Control," AIAA Guidance, Navigation and Control Conference and Exhibit, April 2008.

[5]"Ascending Technologies," `http://www.asctec.de`.

[6]Altug, E., Ostrowski, J., and Taylor, C., "Control of Quadrotor Helicopter Using Dual Camera Visual Feedback," *The Int. Journal of Robotics Research*, Vol. 24, (5), May 2005, pp. 329–341.

[7]Gerig, M., *Modeling, Guidance, and Control of Aerobatic Maneuvers of an Autonomous Helicopter*, Ph.D. thesis, ETH Zurich, 2008.

[8]Michael, N., Mellinger, D., Lindsey, Q., and Kumar, V., "The GRASP multiple micro UAV testbed," *IEEE Robotics and Automation Magazine*, 2010.

[9]Mellinger, D., Michael, N., and Kumar, V., "Trajectory Generation and Control for Precise Aggressive Maneuvers with Quadrotors," Int. Symposium on Experimental Robotics, December 2010.

[10]"Vicon MX Systems," `http://www.vicon.com/products/viconmx.html`.

[11]Quigley, M., Gerkey, B., Conley, K., Faust, J., Foote, T., Leibs, J., Berger, E., Wheeler, R., and Ng, A., "ROS: an open-source Robot Operating System," Open-source software workshop of the Int. Conf. on Robotics and Automation, 2009.

[12]Asbeck, A. T., Kim, S., and Cutkosky, M. R., "Scaling hard vertical surfaces with compliant microspine arrays," Robotics: Science and Systems, June 2005.

[13]Provancher, W., Clark, J., Geisler, B., and Cutkosky, M., "Towards penetration-based clawed climbing," , 2004.

[14]Weiss, L. E., Merz, R., Prinz, F. B., Neplotnik, G., Padmanabhan, P., Schultz, L., and Ramaswami, K., "Shape deposition manufacturing of heterogeneous structures," *Journal of Manufacturing Systems*, Vol. 16, (4), 1997, pp. 239 – 248.

[15]Shen, S., Michael, N., and Kumar, V., "Personal Communications," University of Pennsylvania, Manuscript in preparation, 2010.